Journal of Drug Delivery Science and Technology 80 (2023) 104100

Contents lists available at ScienceDirect

Journal of Drug Delivery Science and Technology

journal homepage: www.elsevier.com/locate/jddst

Green Nanotechnology as an innovative drug delivery approach for *Typha capensis* and Naringenin—New class of phytochemical embedded biocompatible gold nanoparticles in prostate cancer therapy

Keenau Pearce [a], Velaphi C. Thipe [b], Ralf R. Henkel [a], Kattesh V. Katti [b,*]

[a] Department of Medical Bioscience, University of the Western Cape, Cape Town, South Africa
[b] Institute of Green Nanotechnology and Cancer Nanotechnology, Department of Radiology, University of Missouri, Columbia, USA

ARTICLE INFO

Keywords:
Typha capensis
Naringenin
Drug delivery
Prostate cancer
Green nanotechnology

ABSTRACT

Naringenin, a flavone with a growing body of evidence as an anti-cancer agent, is found in *Typha capensis*, an indigenous South African plant commonly used in traditional medicine. However, despite favourable *in vitro* results, clinical usage of naringenin remains restricted due to notoriously poor oral bioavailability, rapid metabolism and poor tumour site availability. This study aimed to investigate a simple, easily reproduced, reliable and effective drug delivery method of mitigating these issues using green nanotechnology principles, and assess their biomedical applications in the treatment of prostate cancer. Gold nanoparticles (AuNPs) were synthesized using green nanotechnology principles and characterized by spectrophotometry, dynamic light scattering, zeta potential, transmission electron microscopy, and Folin-ciocalteu phenol assay. Effects on LNCaP and PC-3 cell viability were evaluated using the MTT assay. A significant ($P < 0.0001$, $P = 0.0003$, $P = 0.0002$) reduction in cell viability was observed for S1-AuNPs, S2-AuNPs and Ng-AuNPs, respectively, in PC3 cells. The extracts, naringenin, and subsequent AuNPs yielded comparable levels of toxicity toward the LNCaP cells. This study reports the first successful synthesis of self-stabilized AuNPs from naringenin in isolation and, most importantly, the application of these novel particles as an effective drug delivery tool. The biomedical applications of this novel formulation and drug delivery approach is expected to aid effective delivery of anticancer therapeutics, in this case naringenin, and thus expand the realms of the treatment of prostate cancer.

1. Introduction

Traditionally, indigenous South African cultures have prepared decoctions from *Typha capensis* (*T. capensis)* rhizomes for medicinal preparations, aimed at the treatment of dysmenorrhea, diarrhoea, venereal disease, and as the name "love reed" suggests, to boost libido and treat fertility disorders in men [1,4]. In contrast to this, early scientific studies into the effects of *T. capensis* extracts on male fertility reported several deleterious effects *in vitro*, namely reduced sperm motility, vitality, sperm reactive oxygen species production, and mitochondrial membrane potential [4,21]. More recently, however, a study investigating the effects of *T. capensis* F1 fractions, produced from seasonal harvests, strongly increased the production of testosterone in TM3 Leydig cells, suggesting a possible application in the treatment of male infertility [23,24]. More importantly, they reported that *T capensis* extracts produced from summer harvests significantly reduced cell viability, induced apoptosis, and yielded DNA fragmentation in the prostate cancer LNCaP cell line while remaining virtually non-toxic toward the non-cancerous TM3 Leydig and PWR-1E benign prostatic hyperplasia cell lines [23,24]. Subsequently, naringenin was identified as one of the bioactives in *T capensis* extracts and credited with a great deal of the reported effects toward prostate cancer cells [23]. These findings are remarkable, given the recent classification of prostate cancer as the second leading cause of cancer-related deaths in men [47]. However, while these studies elucidated valuable insight into the plant's bioactivity, some limitations have been observed. For example, the exact month of collection within the summer harvest was not specified, and considering that varying external environmental factors are known to alter secondary plant compound production [45], this may present a problem when extracts are presented as a therapeutic. Precision is,

* Corresponding author.
E-mail addresses: keenau.pearce@gmail.com (K. Pearce), vctqnf@health.missouri.edu (V.C. Thipe), rhenkel@uwc.ac.za (R.R. Henkel), KattiK@health.missouri.edu (K.V. Katti).

https://doi.org/10.1016/j.jddst.2022.104100
Received 30 September 2022; Received in revised form 13 December 2022; Accepted 19 December 2022
Available online 23 December 2022

therefore, necessary to limit variability and thereby maintain biomedical effectiveness. Moreover, despite promising results under *in vitro* conditions, the *in vivo* usage of isolated naringenin is limited due to poor water solubility [17], variable oral bioavailability depending on the method of delivery [17,42], and rapid metabolism [44] and overall lack of effective drug delivery. Therefore, it is imperative to develop innovative drug delivery approaches so that the tremendous clinical value of these and related phytochemicals can be fully reaped while mitigating the aforementioned limitations.

Apart from naringenin, *T. capensis* rhizome extracts contain several other flavones, phenolic compounds, long-chain hydrocarbons, and various triperpenoids, containing afzelechin, epiafzelechin, catechin, epicatechin, and two novel phenolic compounds known as typharin and typhaphthalide [40]. These are likely the driving force behind the previously reported antioxidant capacity [22]. Phytochemicals with strong antioxidant capacities, such as catechin and epicatechin, have become increasingly popular non-toxic agents in gold nanoparticle (AuNP) synthesis, often playing dual roles as both reducing and stabilizing agents [9,11,14,35]. Furthermore, many of these nanoparticles functionalized with phytochemicals exhibit excellent biocompatibility and notable cytotoxic action toward multiple cancer cell lines [2,3,6,18,26,27,29,30,41,43,49,51], making them promising therapeutic agents in the emerging field known as nano-medicine.

Significant examples of innovative drug delivery approaches, through green nanotechnology, include pioneering efforts by Katti et al. who have performed groundbreaking research and product development focused on the application of green nanotechnology for the scientific rigour and validation of Ayurvedic Medicine [2,3,18,26,27,29,41,49,51]. In this context, the invention of a new medical modality, by Katti and co-workers, referred to as Nano Ayurvedic Medicine has been recently approved by the US Patents and trademarks office [2,3,18,26,27,29,41,49,51]. In a recent report, Katti and co-workers have described outcomes of the first-ever clinical trial investigation for the safety, efficacy and effective drug delivery of AuNPs-based Nano Ayurvedic medicine for treating triple-negative breast cancer patients [29]. This is the first credible scientific rationale toward the application of green nanotechnology-based AuNPs (referred to according to Ayurvedic Modality as Nano Swarna Bhasma), showing effective drug delivery, and widespread utility in oncology for treating various human cancers [29,30]. In a recent publication, Katti et al. have described a complete mechanistic overview on how Nano Swarna Bhasma derived from Mangiferin functionalized AuNPs can be used in the immunotherapy of cancer by targeting and drug delivery to the tumour microenvironment [30]. This is the first-ever scientific investigation showing the unique immune-modulating power of Nano Swarna Bhasma for down-regulating NF-κB. Nuclear factor kappa-light-chain-enhancer of activated B cells (NF-κB) which is found in all types of mammalian cell types is involved in cellular responses to stimuli such as stress, cytokines, and free radicals. It is a protein complex that controls transcription of DNA, cytokine production and cell survival. Extensive investigations have revealed that NF-κB is linked to various cancers, inflammatory and autoimmune diseases, septic shock, viral infection, and improper immune development. Therefore, the recently reported investigations on the ability of Mangiferin functionalized AuNPs in suppressing the activities of NF-κB in tumour cells provide clear clinical evidence on the extraordinary utility of Nano Ayurvedic medicines in treating various human tumours [30]. These investigations also demonstrated the ability of Mangiferin functionalized AuNPs—referred to as Swarna Bhasma in re-educating and modifying the macrophage axis for the transformation of pro-tumor M2 macrophages into the anti-tumour M-phenotypes—thus aiding cancer treating through direct targeting of the tumour microenvironment [30].

Moreover, Katti and co-workers have also recently emphasized the considerable biomedical application of AuNPs as drug-delivery systems due to their unique properties; including a favourable surface area to volume ratio, excellent biocompatibility, propensity toward tumour micro-environment infiltration, and ease of surface modification and functionalization with numerous biomolecules—including proteins, targeted ligands, and chemotherapeutic drugs [50]. For example, studies investigating AuNP-based delivery systems for chemotherapeutics, such as doxorubicin, bleomycin and methotrexate, demonstrated improved cell-specificity, higher intracellular accumulation, and markedly improved cytotoxicity toward drug-resistant cancer cells upon loading the drugs onto AuNPs, in comparison to the unbound drug [15,52,53]. Notably, AuNP-conjugation has also been shown to greatly improve drug delivery, and therefore therapeutic potential, of flavonoids as anti-cancer agents in both *in vitro* and *in vivo* models [16,53].

These findings clearly demonstrate the growing application of phytochemical-functionalized AuNPs in the realm of nano-medicine and cancer therapy, along with their unique potential as drug and phytochemical delivery agents. For all the aforementioned reasons, herein, we have performed the syntheses of AuNPs encapsulated with a cocktail of phytochemicals from *T. capensis* extracts, and naringenin in isolation. The overall objective was to validate our hypothesis that these phytochemical embedded-AuNPs serve as superior drug delivery agents. To evaluate this, the characterization, development, and therapeutic analysis of a self-stabilized drug delivery particle, embedded with naringenin and the plethora of phytochemicals found within *T capensis* extracts formed the major objective of this study.

2. Materials and methods

Unless otherwise noted, all chemicals and reagents were purchased from Sigma-Aldrich Chemical Company (St Louis, MO, USA), and Thermofisher Scientific (Waltham, MA, USA).

2.1. Extract preparation and analysis

Extracts were prepared by the previously described methodology [23,24]. In short, *T. capensis* rhizomes were collected during the summer months and on the Cape Nature Reserve, located in the suburb of Belhar in the Western Cape province of South Africa. Once collected, the rhizomes were washed thoroughly, dried at 25 °C in an air oven, and milled into a fine powder. Next, powdered rhizomes were infused in distilled water heated to 75 °C for 1 h and filtered. The filtrate was then frozen at −80 °C and finally freeze-dried to yield water-soluble extracts. This procedure was performed for samples collected in January and in March, yielding two distinct extracts, labelled *T. capensis* extract sample 1 (S1) and sample 2 (S2), respectively.

2.2. LC-MRM analysis

Samples were dissolved with 1 ml of a solution consisting of 50% methanol, 50% water, 0.01% formic acid and containing 25 ng/ml chloramphenicol. Once dissolved, samples were vortexed for 5 min, then centrifuged 16,000×*g*, and finally, 200 μl transferred into autosampler vials. Supernatants were diluted 1:10, 1:1000 and 1:1000 with chloramphenicol. Next, standards were diluted in methanol to yield a 500 μg/ml working solution and serial diluted 1:1 to concentrations ranging from 200 μg/ml to 1.5625 μg/ml. Finally, standard curves were generated for naringenin. The S1 and S2 extracts, S1-AuNPs, S2-AuNPs and Ng-AuNPs were analyzed using a Xevo TQS mass spectrometer (Waters, Milford MA, USA) with chloramphenicol as internal standard. Naringenin was used as standard.

The Xevo TQS was operated in negative-ion mode. Two transitions were used for each molecule, based on optimized cone and collision generated by the Xevo instrument. Separation was carried out using an Acquity H-class UPLC (Waters) on a Waters BEH C18 column by gradient delivery (0.4 ml/min) of solvent (0.01% formic acid in water and Solvent 0.01% FA in acetonitrile). The total run time was 4 min. The column was heated to 45 °C and the samples cooled to 20 °C in the autosampler. TargetLynx version 4.1 (Waters, Milford MA, USA) was

used to calculate the area under the curve (AUC) and reported as both a response (AUC-compound/AUC-internal standard) and as ng/ml. To quantify naringenin, the linear response function was calculated and the line equation was used to calculate ng/mL from the peak integration data exported from TargetLynx.

2.3. Green synthesis of AuNPs

2.3.1. S1-AuNP and S2-AuNP synthesis

Synthesis was performed using the S1-extract and the S2 extracts with the inclusion of gum arabic (GA). Briefly, 3 mg of GA was added to 3 ml of distilled water and stirred continuously for 30 min at 50 °C. Next, the heat was switched off and 4 mg of the appropriate extract was added and allowed to dissolve for 10 min. Finally, 50 μl of a 0.1 M sodium tetrachloroaurate ($NaAuCl_4$) solution was added in a drop-wise fashion, and the mixture was allowed to stir continuously at ambient temperature for 24 h before characterization.

2.3.2. Ng-AuNP synthesis

Naringenin purchased from Sigma-Aldrich Chemical Company (St Louis, MO, USA) was used for the synthesis of the Ng-AuNPs, and was performed without the inclusion of GA. Briefly, 3 mg of naringenin was added to 3 ml of distilled water and stirred continuously at ambient temperature. Finally, 50 μl of a 0.1 M $NaAuCl_4$ solution, adjusted to pH 8 using a 0.2 M sodium hydroxide solution, was added in a drop-wise fashion, and the mixture was allowed to stir continuously for 24 h before characterization.

2.4. Characterization of AuNPs

The optical properties of each nanoparticle formulation were measured in the 500–600 nm range using a Cary 60 UV–vis spectrophotometer (Agilent Technologies, Santa Clara CA, USA). Dynamic light scattering (DLS) and zeta potential were measured by Zetasizer Nano ZS (Malvern Panalytical, Worcestershire, UK), and core size was determined by transmission electron microscopy (TEM), using a JEOL 1400 transmission electron microscope (JEOL, Tokyo, Japan). TEM images were processed using the java-based processing software ImageJ version 1.8.0 (National Institutes of Health, USA) to calculate particle size distribution. *In vitro* stability was determined using the Cary 60 UV–vis spectrophotometer. Total phenolic concentration for each nanoparticle formulation was measured using the Folin-ciocalteu phenol (FC) method.

2.5. Optical properties, dynamic light scattering and zeta-potential

The optical properties of each nanoparticle formulation were measured, particularly in the 500–600 nm range, using a Cary 60 UV–vis spectrophotometer (Agilent Technologies, Santa Clara CA, USA). The hydrodynamic size and zeta potential were measured by Zetasizer Nano ZS (Malvern Panalytical, Worcestershire, UK) following established methodology [25,29,43,49] In short, 200 μl of each respective nanoparticle formulation were diluted in 800 μl of distilled water (pH 7), to a final volume of 1 ml. For measuring DLS, samples were transferred to a standard disposable cuvette, and to a disposable folded-capillary cell to measure zeta-potential. Hereafter, samples were analyzed using the Zetasizer Nano ZS. An average of 3 measurements were taken.

2.6. Total phenolic quantification

Total polyphenolic concentration was determined according to previously described methodology [49], and was expressed as μg/ml, equivalent to a gallic acid standard curve (500, 250, 125, 62.5, 31.25, 15.62, 7.18, 3.9 and 1.95 μg/ml). Briefly, 1 ml of each respective sample was transferred to a 2 ml centrifuge tube and centrifuged at 15×*g* for 15 min to yield a pellet. Once pelleted, the supernatants were removed from each tube and 500 μl of the Folin-ciocalteu phenol reagent, diluted 1:10 in distilled water, was added to each pellet, followed by 1 ml of a 7.5% (w/v) sodium carbonate solution. Hereafter, samples were briefly mixed and incubated at 30 °C for 30 min. Next, absorbance was determined at 760 nm using the SpectraMax M2 microplate reader (Molecular Devices, San Jose, USA).

2.7. Transmission electron microscopy (TEM)

The core size was determined by TEM. In short, 20 μl of each respective AuNP sample was placed onto a copper gilder grid (Electron Microscopy Sciences) and allowed to air-dry. Finally, grids were viewed, using a Joel 1400 transmission electron microscope (JEOL, Tokyo, Japan). The java-based processing software ImageJ version 1.8.0 (National Institutes of Health, USA) was subsequently used to measure individual particle size.

2.8. In vitro AuNP stability

In vitro AuNP stability was investigated using previously established methodology [25,43,49]. In short, this was achieved by combining 200 μl of each nanoparticle formulation and 800 μl of each challenging medium, specifically 1% sodium chloride, 0.2% histidine, 0.5% human serum albumin (HSA), 0.5% bovine serum albumin (BSA), 0.5% cysteine and phosphate buffered saline (PBS) solution, to a final volume of 1 ml, respectively. Controls were combined with distilled water. Each mixture was incubated for 24 h. Finally, AuNP stability was measured by recording optical properties, particularly absorption maxima (λ_{max}) using UV–vis spectrophotometry.

2.9. In vitro effects of AuNPs on prostate cancer cells

The LNCaP and PC-3 prostate cancer cell lines were used for this study. They were cultivated at 37 °C in 95% air and 5% CO_2, following standard aseptic work procedures. LNCaP and PC-3 cells were cultured in complete RPMI 1640 growth medium, supplemented with 10% fetal bovine serum, 1% penicillin (100 IU/ml) and streptomycin (100 μg/ml), in 25 cm^2 culture flasks.

2.9.1. Cell viability MTT assay

The effects of each extract and AuNP toward LNCaP and PC-3 prostate cancer cell viability were determined using the 3-(4,5-dimethylthiazolyl-2)-2, 5-diphenyltetrazolium bromine (MTT) cell proliferation assay over 24 and 72 h periods. Briefly, cells were seeded into 96-well polystyrene plates at 5×10^3 cells/well in 100 μl of complete growth medium and allowed to adhere. Next, cells were treated with varying concentrations (200, 100, 50, and 12.5 μg/ml) of the extracts and AuNPs for 24 h and 72 h, respectively. Next, 10 μl of MTT were added to each well and plates were incubated at 37 °C for an additional 4 h. Growth medium and MTT were removed from each well, the remaining crystals were solubilized with 200 μl of dimethylsulphoxide (DMSO), and absorbance was measured at 570 nm using the SpectraMax M2 microplate reader (Molecular Devices, San Jose, USA). Results were expressed as percentage viability using the following formula: % viability = (T/C) x 100%, where C = absorbance of control and T = absorbance of treated cells.

2.10. AuNP internalization by dark field microscopy

AuNP internalization by dark field microscopy [49]. In short, LNCaP and PC-3 cells were seeded over coverslips in sterile 6-well plates at 5×10^5 cells/well in 2 ml of complete RPMI 1640 and incubated for 24 h at 37 °C in 95% air and 5% CO_2. Cells were treated with 50 μg/ml concentrations of the S1-AuNPs, S2-AuNPs and the Ng-AuNPs for 24 h, respectively. Thereafter, cells were washed 10 times with PBS and fixed using 4% paraformaldehyde for 15 min at room temperature. The

fixative was then removed and cells were washed 3 times with PBS. To prepare the slides, coverslips were removed from the 6-well plates, inverted, mounted with DAPI (stain nuclear) on glass slides and allowed to incubate at room temperature for 10 min. Finally, staining was observed using a dark field microscope capable of hyperspectral imaging technology (CytoViva), where the presence of AuNPs was observed as yellow-gold coloured particulates or agglomerates found covering or surrounding the blue-stained cells.

2.11. AuNP internalization by TEM

AuNP internalization by TEM was investigated using previously established methods [49]. In short, PC-3 cells were seeded over coverslips in sterile 6-well plates at 5×10^5 cells/well in 2 ml of complete RPMI 1640. Cells were treated with 50 and 100 μg/ml concentrations of the S1-AuNPs, S2-AuNPs and the Ng-AuNPs, over 6 and 24-h periods, respectively. Thereafter, cells were washed 10 times with PBS and dislodged with 300 μl of 0.25% trypsin. Hereafter cells were centrifuged at 125×*g* to form a pellet, supernatants removed, and cell pellets washed with PBS and centrifuged once more at 125×*g*. Subsequently, the PBS was removed and carefully replaced with TEM fixative (100 mM sodium cacodylate, 2% glutaraldehyde and 2% paraformaldehyde), without disturbing the cell pellet and stored at 4 °C. Finally, the fixed cell pellets were used for grid preparation and viewed using a transmission electron microscope (Joel 1400).

2.12. Statistical analysis

Data were recorded and analyzed statistically using MedCalc for Windows, version 19 (MedCalc Software, Mariakerke, Belgium). Data were tested for normality and analyzed further using the independent *t*-test and one-way ANOVA. A P-value of less than 0.05 was considered significant.

3. Results

3.1. Extract analysis

Levels of naringenin were quantified in each *T. capensis* extract (S1 and S2) using LC-MRM analysis (Fig. 1). A clear discrepancy was observed between the S1-extract and S2-extract. Naringenin was found to be higher in the S1-extract, accounting for 171.2 ng/ml, and lower in the S2 extract (Fig. 1b), accounting for 86.6 ng/ml.

3.2. Synthesis and in vitro stability of AuNPs

Upon reaction, distinct colour shifts within the red-purple spectrum were observed, namely a shift from yellow-brown to a deep violet within 1 h for the S1 and S2-extracts, and a gradual shift from milky white to deep ruby over 24 h for naringenin. Furthermore, UV–vis spectroscopic analysis demonstrated peak absorbance in the 500–550 nm range (Fig. 2), namely 540 nm for the S1-AuNPs (Figs. 2a), 534 nm for the S2-AuNPs (Figs. 2c), and 540 for the Ng-AuNPs (Fig. 2e).

Stability was assessed by incubating each AuNP with various blood-mimicking components, namely sodium chloride (NaCl), cysteine, histidine, HSA, BSA, and PBS, over 24 h. Slight increases in λ_{max} were observed in each buffer tested with the S1-AuNPs (Fig. 2b), while the S2-AuNPs (Fig. 2d) yielded marginal decreases. Nevertheless, no major shifts in surface plasmon resonance (SPR) or signs of agglomeration were observed. Conversely, the Ng-AuNPs (Fig. 2f) showed remarkable stability in each buffer tested, with no notable shifts in SPR or signs of agglomeration.

3.3. Dynamic light scattering, zeta potential and total phenolic quantification

Dynamic light scattering (DLS), polydispersity index (PDI) and zeta potential were measured using the Zetasizer Nano ZS (Malvern Panalytical, Worcestershire, UK), and the Folin-ciocalteu phenol (FC) method was utilized to gain insight into the phenolic content of each nano-formulation. These findings are summarized in Table 1.

Average hydrodynamic sizes were below 100 nm for each nano-formulation. The S1-AuNPs measured 88.36 nm with a PDI of 0.284, the S2-AuNPs measured 96.73 nm with a PDI of 0.393, and the Ng-AuNPs measured 29.28 nm with a PDI of 0.685. Zeta-potential measurements revealed strong negative charges for each nano-formulation. S1-AuNPs yielded an average zeta potential of −27.1 mV, the S2-AuNPs yielded an average zeta potential of −29.3 mV, and the Ng-AuNPs yielded an average zeta potential of −33.3 mV. Variations in the calculated total polyphenolic content were noted between each of the gold nanoparticle formulations. A total phenolic concentration of 447 μg/ml was found for the S1-AuNPs, 487 μg/ml 288 μg/ml for the Ng-AuNPs.

3.4. TEM and size distribution

When visualized using TEM (Fig. 3), the S1-AuNPs (Fig. 3a) and S2-AuNPs (Fig. 3c) consisted of a majority of spherically shaped nanoparticles, with a small proportion of triangle-shaped nanoparticles of

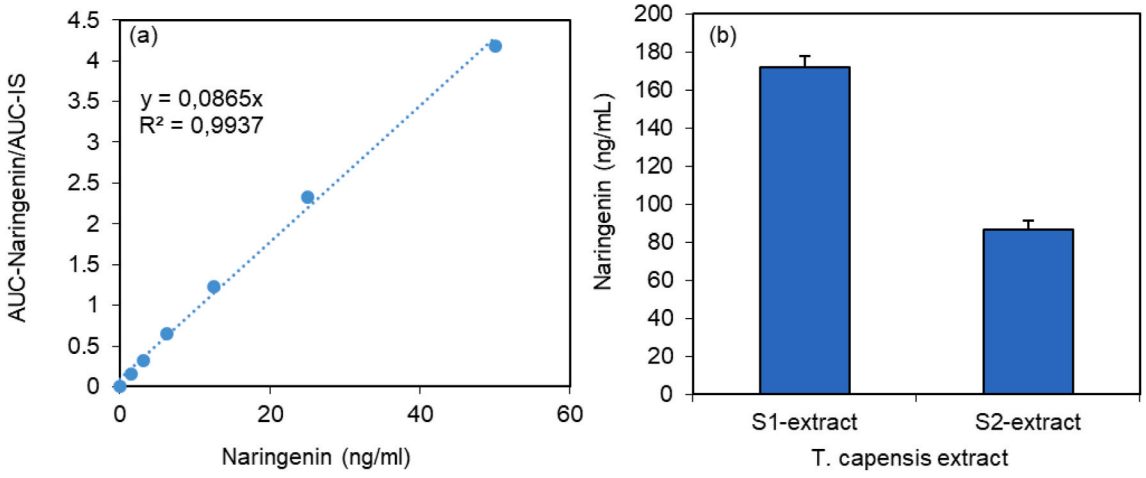

Fig. 1. Naringenin content of the S1 and S2 extract analyzed by LC-MRM. The S1-extract exhibited 171.2 ng/ml of naringenin, while 86.6 ng/ml was found in the S2-extract.

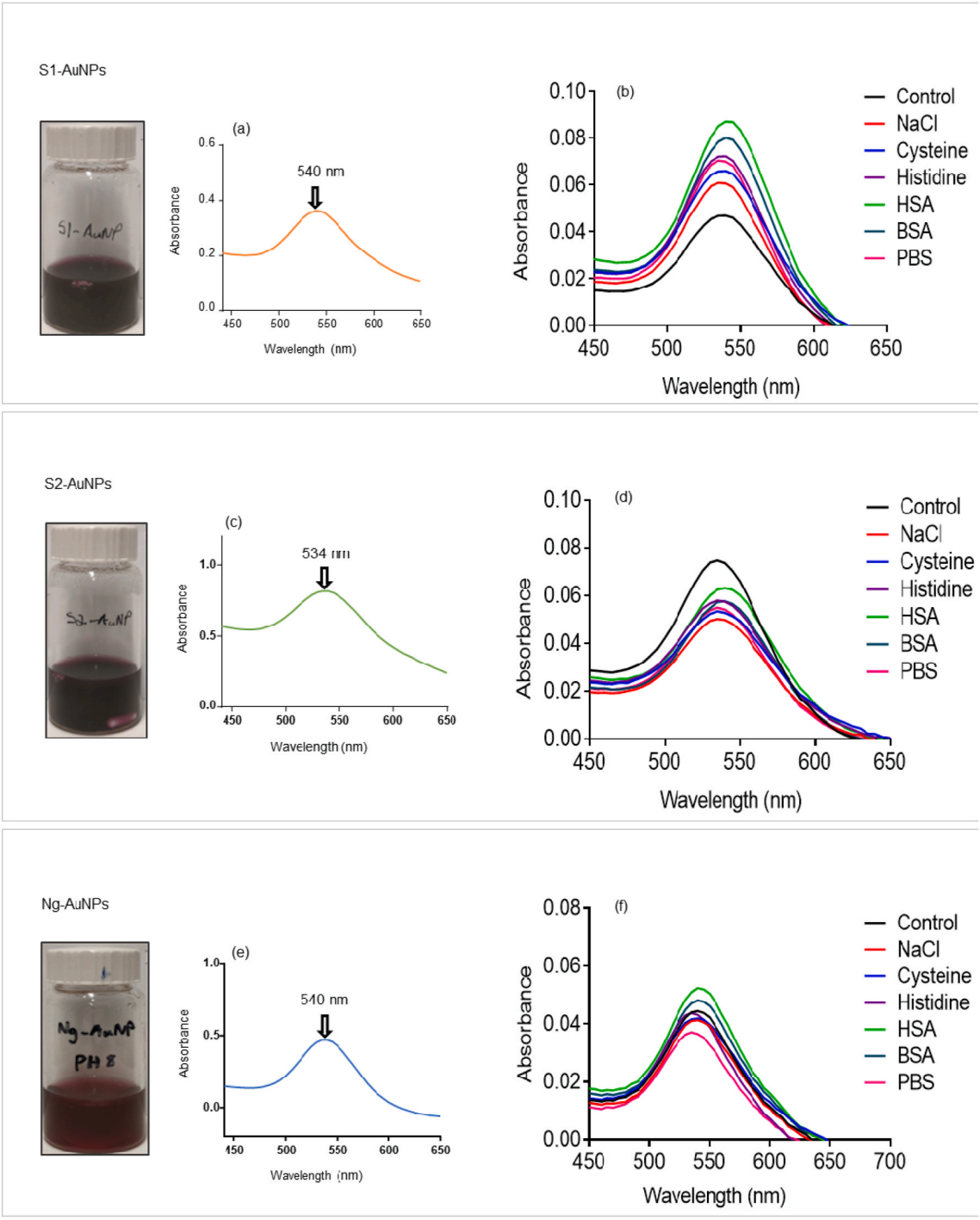

Fig. 2. Spectrophotometric analysis of AuNPS. Absorption maximums are shown for the S1-AuNPs (a), S2-AuNPs (c), and Ng-AuNPs (c). AuNP stability in NaCl, cysteine, histidine, HSA, BSA and PBS are shown for S1-AuNP's (b), S2-AuNP's (d), and Ng-AuNP's (f). AuNPs showed remarkable stability in each challenging media over 24 h.

variable size, and a calculated average particle size of 28.29 nm (Figs. 3b) and 18.99 nm (Fig. 3d), respectively. Conversely, the Ng-AuNPs (Fig. 3e) only presented as spherically shaped particles with a consistent observable size and a calculated average size of 12.53 nm (Fig. 3f).

3.5. PC-3 cell viability

3.5.1. S1-AuNP and S1-extract

Following 24-h exposure to the S1-extract and S1-AuNP's (Fig. 4a), respectively, significant ($P = 0.03$, $P = 0.0001$, $P = 0.0001$) differences between the extract and AuNPs were observed between 50 and 200 μg/ml. One-way ANOVA revealed significant ($P < 0.001$) trends between the control and 200 μg/ml, for both the S1-extract and S1-AuNPs. Over 72 h (Fig. 4b), significant ($P < 0.0001$, $P = 0.0001$, $P < 0.001$, $P < 0.0001$, $P < 0.0001$) differences between 12.5 and 200 μg/ml were observed. Similarly, one-way ANOVA revealed a significant ($P < 0.001$) trend between the control and 200 μg/ml, for the S1-extract and S1-AuNPs.

Table 1
DLS, Zeta-potential and phenolic concentration for the S1-AuNPs, S2-AuNPs and Ng-AuNPs.

Sample	DLS (nm)	PDI	Zeta-Potential (mV)	Calculated phenolic concentration (μg/ml)
S1-AuNP	88.36 ± 1.41	0.284	−27.1 ± 0.20	447
S2-AuNP	95.73 ± 1.93	0.393	−29.3 ± 0.80	487
Ng-AuNP	29.28 ± 0.09	0.685	−33.3 ± 1.31	288

3.5.2. S2-AuNP and S2-extract

After 24 h of exposure (Fig. 5a), significant ($P = 0.0006$, $P = 0.0319$) differences were observed between the S2-extract and S2-AuNPs from 100 to 200 μg/ml. One-way ANOVA revealed significant ($P = 0.001$, $P < 0.001$) trends between the control and 200 μg/ml, for the S1-extract and S2-AuNPs, respectively. Over 72 h (Fig. 5b), significant ($P = 0.0021$, $P = 0.0001$, $P = 0.0004$, $P < 0.0001$, $P = 0.0003$) differences from 12.5 to 200 μg/ml were observed. One-way ANOVA revealed a significant ($P < 0.001$) trend between the control and 200 μg/ml.

3.5.3. Ng-AuNP and naringenin

Following 24-h exposure to naringenin and Ng-AuNPs, respectively (Fig. 6a). Significant ($P = 0.008$, $P < 0.0001$, $P = 0.0069$, $P = 0.0009$) differences were observed between naringenin and Ng-AuNPs at 25 μg/ml, 50 μg/ml, 100 μg/ml and 200 μg/ml. One-way ANOVA revealed significant ($P < 0.001$) trends between the control and 200 μg/ml, for naringenin and Ng-AuNPs. Moreover, significant ($P = 0.0199$, $P = 0.0125$) differences at 100 μg/ml and 200 μg/ml were observed, following 72 h of exposure (Fig. 6b), along with one-way ANOVA revealing significant ($P < 0.001$) trends between the control and 200 μg/ml, for naringenin and Ng-AuNPs.

3.6. LNCaP cell viability

3.6.1. S1-AuNPs and S1-extract

Cells were exposed to the S1-extract and S1-AuNPs over 24 (Fig. 7a). Significant ($P = 0.0048$, $P = 0.0056$, $P = 0.0004$, $P = 0.0123$) differences were observed between the S1-extract and S1-AuNPs at 12.5 μg/ml, 50 μg/ml, 100 μg/ml and 200 μg/ml. One-way ANOVA yielded significant ($P < 0.001$) trends between control-200 μg/ml, for the S1-extract and S1-AuNPs. Over 72 h (Fig. 7b), significant ($P = 0.0001$, $P = 0.0068$, $P = 0.0001$, $P = 0.0033$) differences at 12.5 μg/ml, 25 μg/ml and 100 μg/ml were observed. One-way ANOVA yielded significant ($P < 0.001$) trends between the control and 200 μg/ml, for the S1-extract and S1-AuNPs.

3.6.2. S2-AuNP and S2-extract

After 24 h of treatment with the S2-extract and S2-AuNPs (Fig. 8a), significant ($P = 0.0001$ and $P < 0.0001$) differences were observed between the S2-extract and S2-AuNPs from 25 to 200 μg/ml, respectively. One-way ANOVA yielded significant ($P < 0.001$) trends from control-200 μg/ml, for both the S2-extract and S2-AuNPs, respectively. Moreover, significant ($P = 0.0001$ and $P < 0.0001$) differences were observed at 25 μg/ml and 50 μg/ml, 100 μg/ml and 200 μg/ml after 72 h of exposure (Fig. 8b). One-way ANOVA revealed significant ($P < 0.001$) trends from control-200 μg/ml, for both the S2-extract and S2-AuNPs, respectively.

3.6.3. Ng-AuNP and naringenin

Following 24 h of exposure to naringenin and the Ng-AuNPs, significant ($P = 0.0001$, $P = 0.0003$) differences were observed between naringenin and Ng-AuNPs at 25 μg/ml, and 50 μg/ml and 200 μg/ml, respectively (Fig. 9a). One-way ANOVA yielded significant ($P < 0.001$) trends from control-200 μg/ml, for both naringenin and Ng-AuNPs. Over 72 h (Fig. 9b), significant ($P = 0.0245$) differences were observed at 12.5 μg/ml. One-way ANOVA revealed significant ($P < 0.001$) trends between the control and 200 μg/ml, for both naringenin and the Ng-AuNPs.

3.7. Cell internalization by dark-field microscopy and TEM

Analysis by dark field microscopy in LNCaP (Fig. 10) and PC-3 (Fig. 11) cells demonstrated that the S1-AuNPs, S2-AuNPs and Ng-AuNPs possessed a clear affinity toward LNCaP cells over 6 and 24 h, with large AuNP aggregates covering cell surfaces, with particular regard to cell cytoplasm and nuclei. Similarly, strong cell affinity was observed in PC-3 cells, with each nano-formulation accumulating over cytoplasmic and nucleic cell surfaces indiscriminately. Upon further analysis by TEM (Fig. 12), the S1-AuNPs and Ng-AuNPs were detected intracellularly in PC-3 cells, following 6 (Figs. 12a) and 24 (Fig. 12b) hours of incubation. No signs of agglomeration were observed following internalization.

4. Discussion

4.1. AuNP synthesis and characterization

Both, *T. capensis* extracts and naringenin in isolation yielded an observable colour shift toward a red-purple spectrum upon reaction, with peak absorbance in the 500–550 nm range upon spectroscopic analysis. These factors are highly indicative of successful AuNP synthesis [5,13], which was confirmed by TEM imaging. This comes as no surprise, for the extracts, when the plethora of phytochemicals found within *T. capensis* [40] and antioxidant action [5] are considered. In particular, catechin and epicatechin were previously reported to act as reducing, and sometimes stabilizing agents [9,11,14,35]. It is, thus, possible that a combination of these phytochemicals contributed to the synthesis, and possibly capping, of the extract-derived nanoparticles reported in this study. Conversely, naringenin in isolation does not have a documented history of AuNP synthesis, and its contribution to the formation of the S1-AuNP and S2 AuNP, therefore, remains unclear. Additionally, AuNP synthesis using naringenin in isolation was presently noted to occur only when the pH was adjusted to a range of pH 7–8. Similar reports exist, such as pH adjustment using sodium hydroxide, being paramount to the successful synthesis of uniform AuNPs using carboxymethyl chitosan as a reducing agent [46]. Interestingly, the inclusion of a stabilizing agent, such as GA, was not found to be necessary, suggestive of a naringenin coating on the Ng-AuNP surface.

Further analysis of these AuNPs showed that the S2-AuNPs and Ng-AuNPs each possess a strong negative charge close to and lower than −30 mV, respectively, which typically confers greater repulsive forces, and thus excellent colloidal stability [19,20]. It must be mentioned, however, that the S1-AuNPs exhibited a slightly weaker charge of −27.1 ± 0.20 m V, and thus may have a marginally greater propensity toward agglomeration over time. Moreover, core sizes, as calculated from TEM images, are notably smaller than the reported hydrodynamic sizes, which is a measure of both core and cap-size. This may serve to confirm the capping of AuNPs with a combination of GA and available phytochemicals for the S1-AuNPs and S2-AuNPs, and naringenin in the Ng-AuNPs. This study reports the first known instance of AuNPs synthesis from *T. capensis* extracts coated with a multitude of phytochemicals. Additionally, the first successful synthesis of AuNPs using the flavone naringenin as both a reducing and stabilizing agent is also reported. Considering the medicinal value of *T capensis* extracts and their bioactives, these AuNPs are likely to have exciting novel biomedical applications.

4.2. T. capensis extracts, AuNPs and prostate cancer cells

It is commonplace for a degree of plant compound variation to exist,

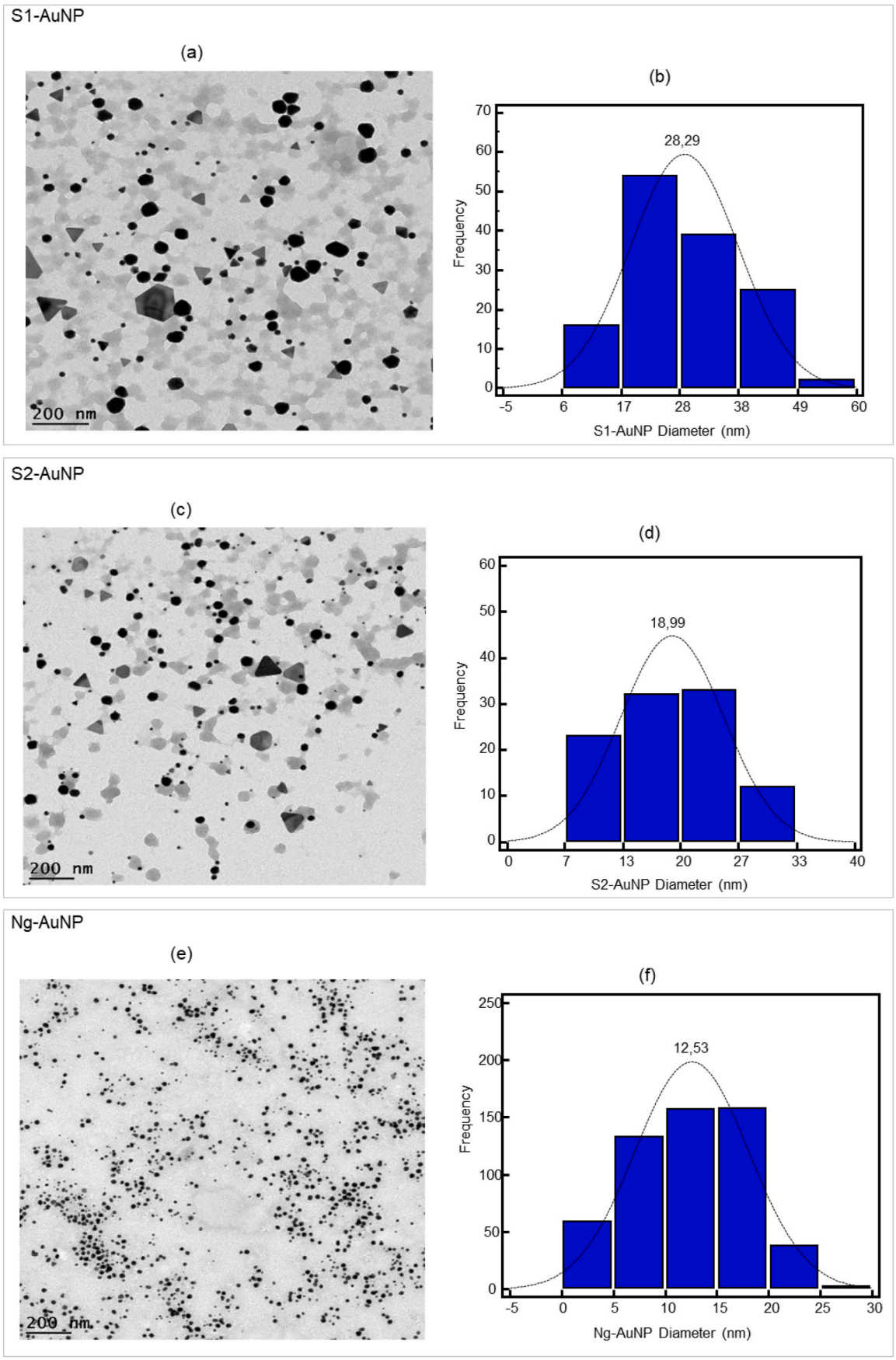

Fig. 3. TEM imaging and size distribution histograms for the S1-AuNPs (a–b), S2-AuNPs (c–d), and Ng-AuNPs (e–f).

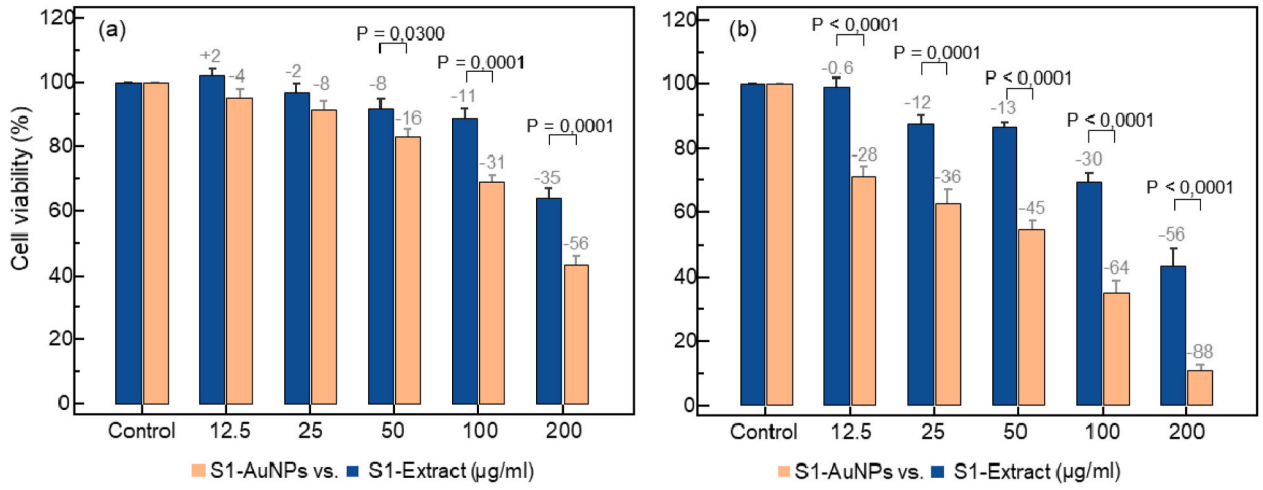

Fig. 4. Effects of S1-extract and S1-AuNPs on PC-3 cell viability as assessed by the MTT assay over 24 (a), and 72 (b) hours of treatment. Dose-dependent decreases in cell viability were noted between control and 200 µg/ml of the S1-extract and S1-AuNPs over both exposure periods.

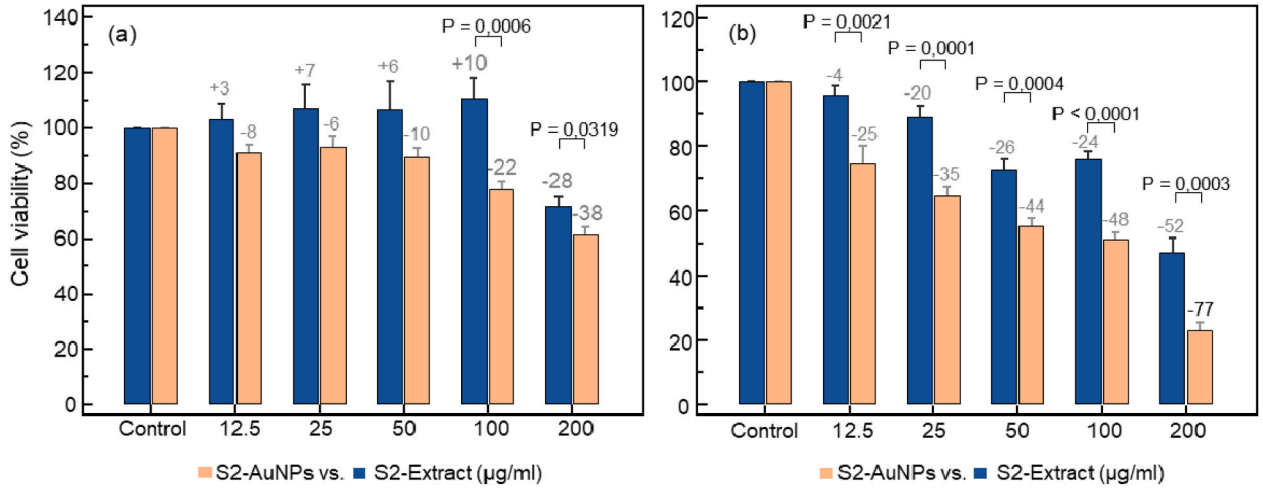

Fig. 5. Effects of S2-extract and S2-AuNPs on PC-3 cell viability as assessed by the MTT assay over 24 (a), and 72 (b) hours of treatment. S2-AuNPs produced dose-dependent decreases in cell viability between control and 200 µg/ml over 24 h (a). Over 72 h (b), both the S1-extract and S2-AuNPs each dose-dependent reduction in cell viability control and 200 µg/ml.

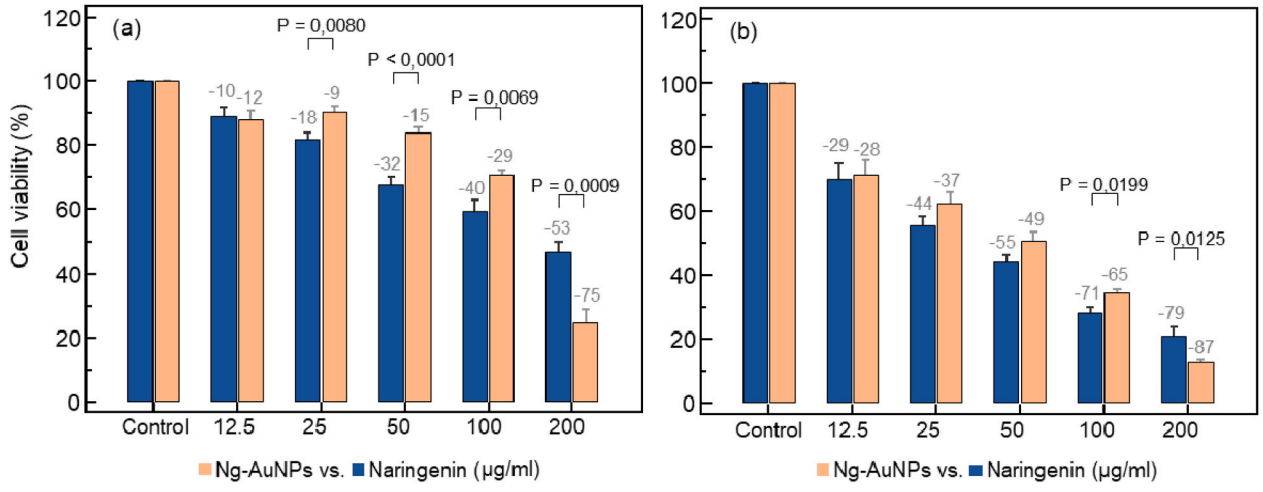

Fig. 6. Effects of naringenin and Ng-AuNPs on PC-3 cell viability determined by the MTT assay following 24 (a), and 72 (b) hours of treatment. Cell viability was reduced comparably at each concentration over 24 (a) and 72 (b) hours.

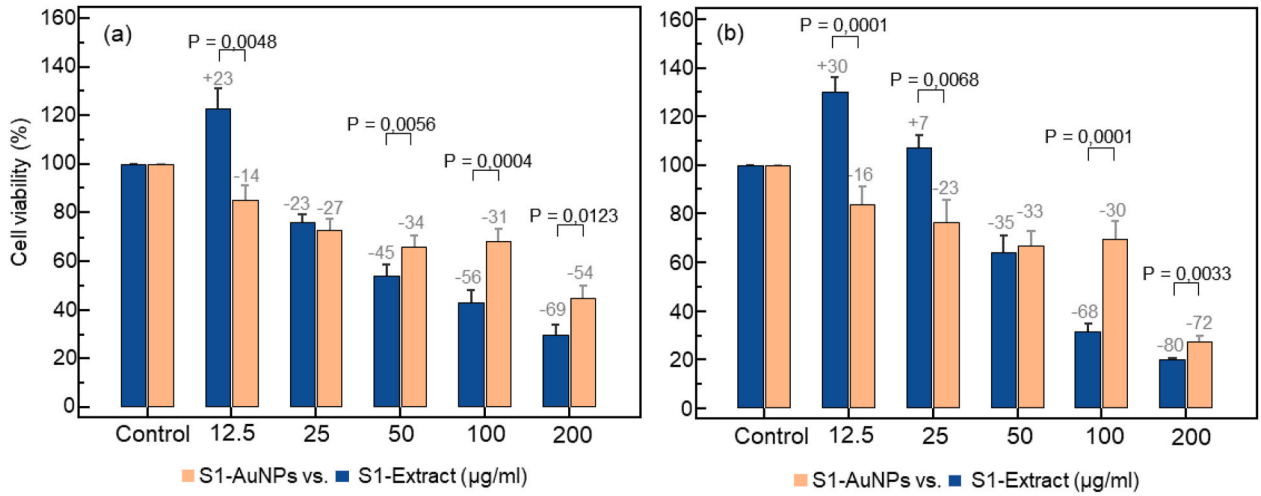

Fig. 7. Effects of S1-extract and S1-AuNPs on LNCaP cell viability as measured by the MTT assay following 24 (a), and 72 (b) hours of treatment. Cell viability was reduced dose-dependently at each concentration, with the S1-AuNPs yielding significantly (P = 0.0004, P = 0.0123, P = 0.0001 and P = 0.0033) greater reductions at higher concentrations over 24 (a) and 72 (b) hours, respectively.

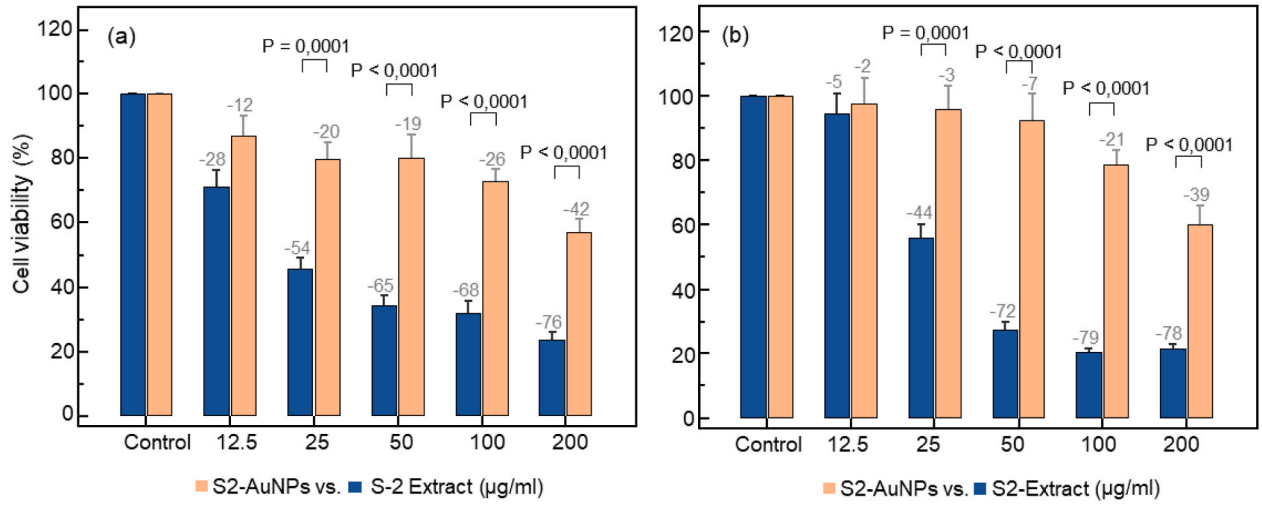

Fig. 8. Effects of S2-extract and S2-AuNPs on LNCaP cell viability as assessed by the MTT assay over 24 (a), and 72 (b) hours of treatment. Significantly (P < 0.0001) greater, dose-dependent reductions in cell viability were noted for the S2-extract at each concentration tested over 24 (a) and 72 (b) hours of treatment.

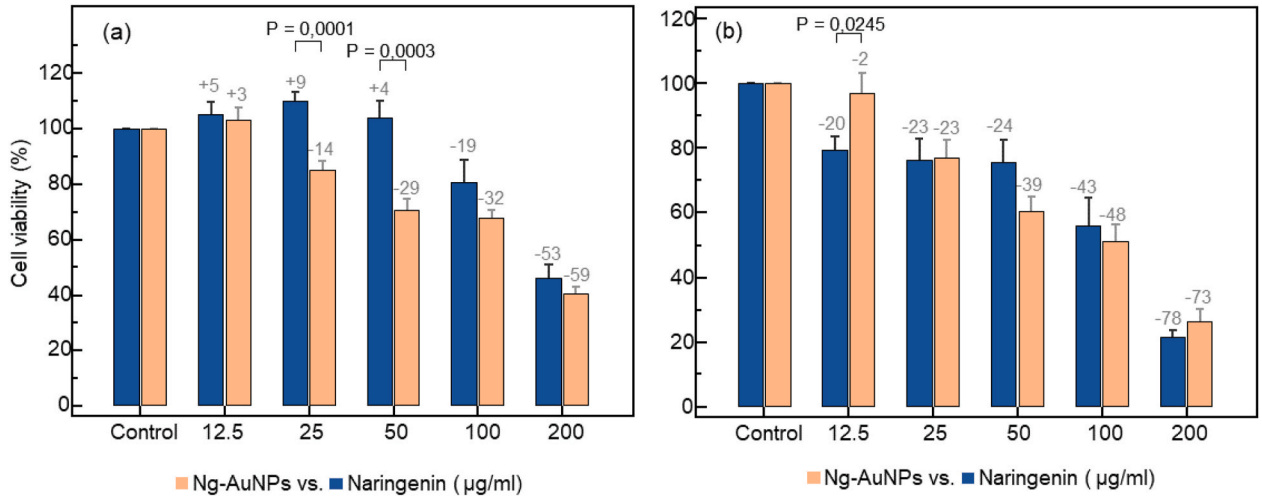

Fig. 9. Effects of naringenin and Ng-AuNPs on LNCaP cell viability determined using the MTT assay over 24 (a), and 72 (b) hours of treatment. Comparable cytotoxic effects were observed between the naringenin and the Ng-AuNPs at each concentration tested.

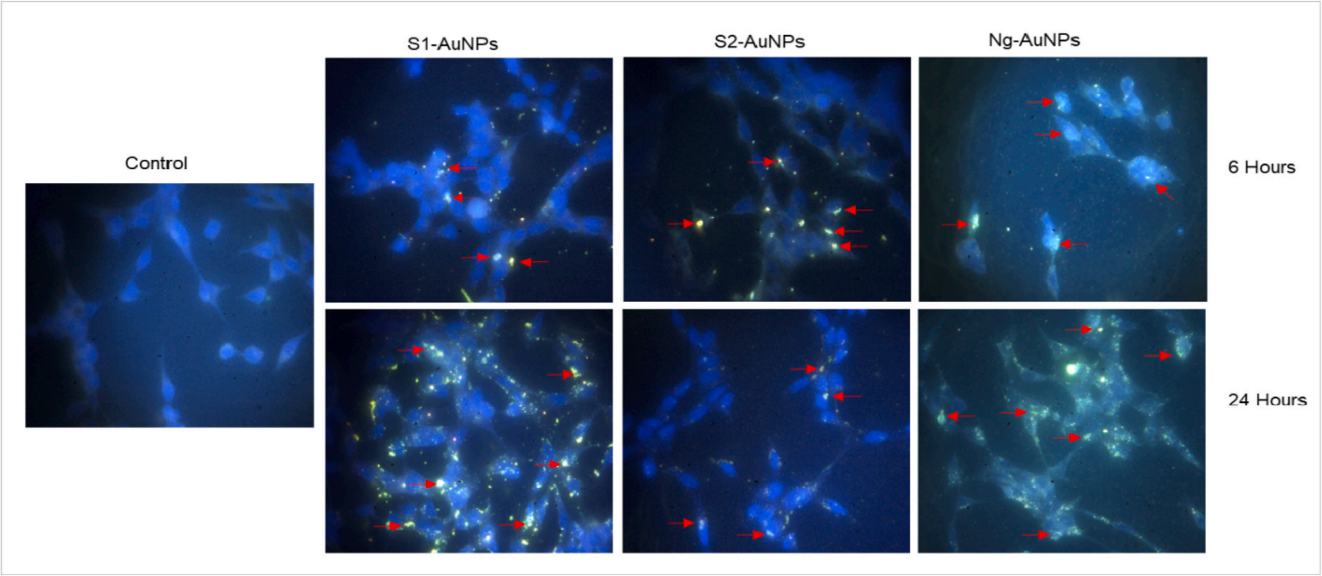

Fig. 10. Cell internalization by dark field microscopy in LNCaP cells following 6 and 24 h of incubation with 100 μg/ml of the S1-AuNPs, S2-AuNPs, and Ng-AuNPs, respectively. Notable instances of possible internalization were seen for each AuNP and are marked by red arrows. (For interpretation of the references to colour in this figure legend, the reader is referred to the Web version of this article).

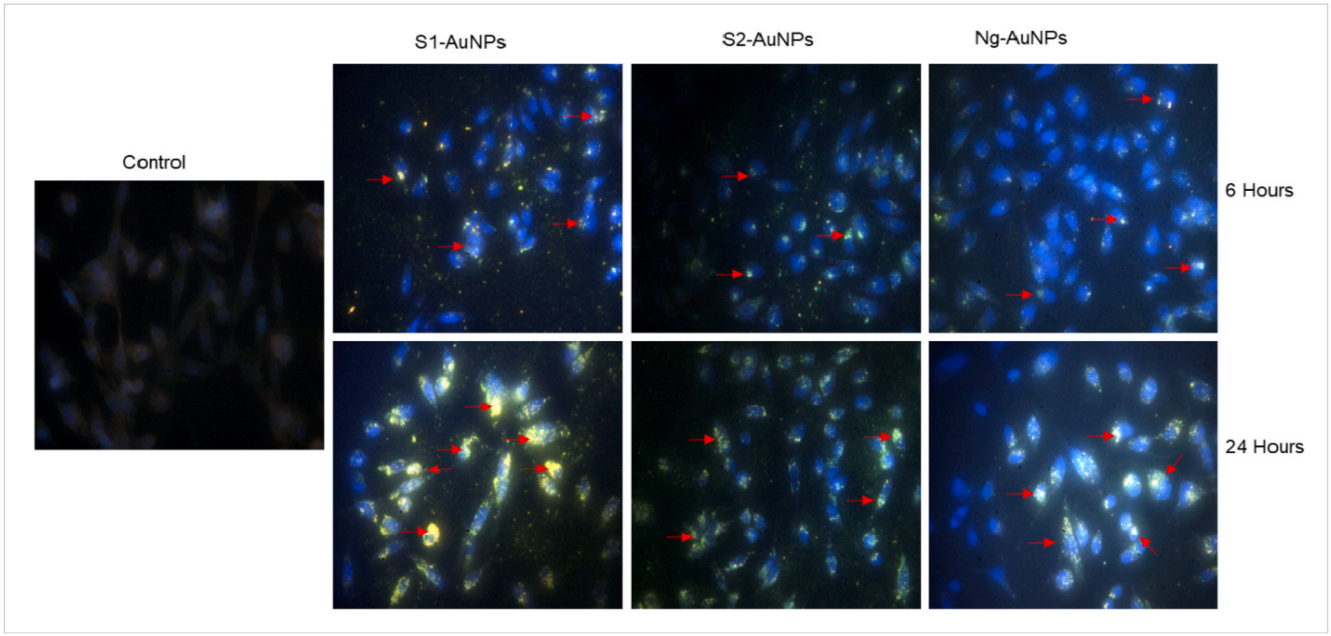

Fig. 11. Cell internalization by dark field microscopy in PC-3 cells following 6 and 24 h of incubation with 100 μg/ml of the S1-AuNPs, S2-AuNPs, and Ng-AuNPs, respectively. Notable instances of possible internalization were seen for each AuNP and are marked by red arrows. (For interpretation of the references to colour in this figure legend, the reader is referred to the Web version of this article).

especially when a comparison is drawn between geographical locations, external environmental factors, and seasons [39,45,54]. In this study, a clear discrepancy in overall bioactive concentration was found when plant material was collected at different points within the summer season, and subsequent extracts were analyzed. Despite this, however, both extracts were found to yield comparable, dose- and time-dependent reductions in LNCaP and PC-3 cell viability. It is therefore clear that the varying overall concentration of naringenin was not found to hold any significant influence over their cytotoxic effects toward prostate cancer cells. These findings corroborate the previously reported effect of bioactivity toward LNCaP cells [10,23,33], and further suggest that the medicinal value of *T. capensis* extracts toward prostate cancer may not be governed by the specific quantity of naringenin, but simply the overall presence. Therefore, plant collection within the summer season is sufficient to maintain the medicinal value of the extract, when intended as a therapeutic in the treatment of prostate cancer. By comparison, the extract-derived AuNPs produced varying levels of toxicity toward LNCap and PC-3 cells.

In LNCaP cells, it was found that the S1-AuNP produced dose- and time-dependent toxicity comparable to the S1-extract, while the S2-AuNPs were observably less toxic than the S2-extract. In PC-3 cells, however, both the S1-AuNPs and S2-AuNPs yielded higher levels of overall toxicity as compared to their extract counterparts—thus providing stellar proof of the importance of green nanotechnology in

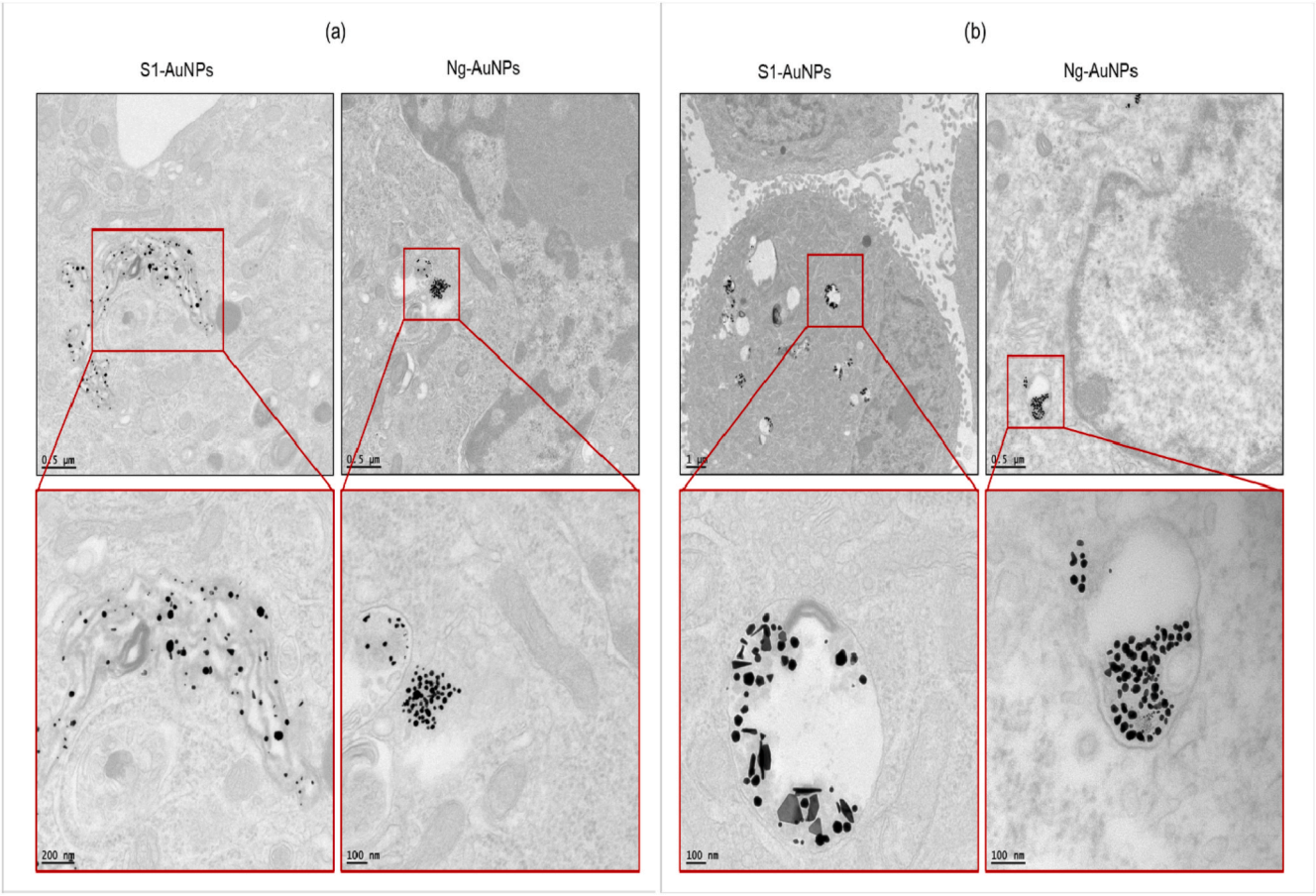

Fig. 12. Internalized AuNPs imaged by TEM in PC-3 cells following 6 (a) and 24 (b) hours of incubation with 100 μg/ml of the S1-AuNPs and Ng-AuNPs, respectively. Both S1-AuNPs and Ng-AuNPs were detected within cells at each time point.

achieving effective drug delivery. Additionally, these findings suggest that the S1-AuNPs and S2-AuNPs may possess a degree of cell-specificity between the LNCaP and PC-3 cells. Furthermore, nano-encapsulating available phytochemicals only appeared to improve therapeutic effects toward PC-3 cells, and not LNCaP cells, suggesting a more suited application in the treatment of late-stage, hormone-independent prostate cancer—which is the most important unmet clinical need requiring urgent therapeutic interventions [31,34,48]. Analysis by dark-field microscopy also demonstrated a greater propensity toward PC-3 cells for both AuNPs, along with TEM imaging confirming the presence of intracellular AuNP in PC-3 cells. These findings further suggest a greater affinity toward PC-3 cells. Considering that naringenin has previously been shown to possess a degree of cell specificity toward PC-3 cells [32], rather than LNCaP, the greater affinity toward PC-3 cells reported here may be explained by the surface-bound naringenin in the extract-derived AuNPs. This may be supported by the action of the Ng-AuNPs.

Presently, the Ng-AuNPs appeared to have favourable effects towards prostate cancer cells, albeit comparable to free naringenin, in LNCaP and PC-3 cells. However, effective drug delivery affording optimum bioavailability of the phytochemical is only feasible when the phytochemicals are bound to gold nanoparticulate surfaces as in Ng-AuNPs, S1-AuNPs and S2-AuNPs. Furthermore, dark-field microscopy also revealed a greater observable affinity toward PC-3 cells, along with subsequent TEM imaging revealing intracellular AuNPs in PC-3 cells. At first glance, the comparable cytotoxicity may appear to offer no biologically significant benefit over free naringenin, but considering the limitations inherent to the flavonoid reveals the true potential of the Ng-AuNPs. Naringenin possesses enormous medicinal potential, ranging from being anti-carcinogenic and anti-inflammatory, to being radiosensitizing [7,8,28,37]. However, its clinical usage is severely limited due to poor water solubility, poor oral bioavailability and intestinal absorption, low stability, rapid metabolism and ineffective transport across biological membranes yielding low tumor site bioavailability [8,17,36–38]. Previous attempts to improve bioavailability and absorption included complexing the flavonoid with β-cyclodextrin to improve uptake [38], forming polymeric nano-suspensions of naringenin [8,36] and binding naringenin to AuNPs synthesized via citrate reduction [8,12]. These methods may improve delivery but are complex, labour-intensive and expensive. Conversely, we report small, highly stable AuNPs synthesized directly from naringenin, using it as a dual reducing and a stabilizing agent. Moreover, the Ng-AuNPs also showed drug delivery effects comparable to free naringenin towards LNCaP and PC-3 cells, likely indicating a similar mode of action. However, the ability of AuNP-bound phytochemicals to withstand enzymatic degradation *in vivo* presents significant prospects for their ultimate use in oncology. Therefore, the present findings signify a simple, and a reliable drug delivery method—through green nanotechnology—thus overcoming the clinical limitations associated with naringenin by AuNP-mediated drug delivery.

5. Conclusions

In this study, our hypothesis that phytochemicals embedded-AuNPs serve as superior drug delivery agents to tumor sites and thus provide significantly improved therapeutic benefits for treating various human cancers has been experimentally validated. This investigation is a major step toward realizing the goal of the World Health Organization (WHO)

which has forecast that the global population would largely embrace herbal medicine for treating various diseases and disorders. More importantly, according to the author's knowledge, this study reports the first successful synthesis of highly stable gold nanoparticles using the bioactive compound naringenin in isolation, serving as a dual reducing and stabilizing agent. Considering enhanced drug delivery features, and toxicity observed with these particles, our findings are expected to have realistic biomedical applications for the treatment of prostate and other cancers, as well as for the wider medical field, particularly in novel disease treatment and management strategies.

Funding

This research was funded by The South African National Research Foundation (NRF) and University of Missouri Institute of Green Nanotechnology.

Author statement

Keenau Pearce: Data curation, Formal analysis, Investigation, Writing- Original draft preparation. Ralf Henkel: Conceptualization, Supervision. Kattesh Katti: Conceptualization, Supervision, Writing-Reviewing and Editing. Velaphi Clement Thipe: Methodology, Formal analysis, Investigation, Validation.

Declaration of competing interest

The authors declare no conflict of interest.

Data availability

Data will be made available on request.

Acknowledgments

The authors thank the South Africa National Research Foundation, the University of Missouri Institute of Green Nanotechnology, where this research was conducted, and the University of Missouri Electron Microscopy Core Facility.

References

[1] H.S. Abdillahi, J. Van Staden, South African plants and male reproductive healthcare: conception and contraception, J. Ethnopharmacol. 143 (2012) 475–480.
[2] A.Y. Al-Yasiri, M. Khoobchandani, C.S. Cutler, L. Watkinson, T. Carmack, C. J. Smith, M. Kuchuk, S.K. Loyalka, A.B. Lugão, K.V. Katti, Mangiferin functionalized radioactive gold nanoparticles (MGF- 198 AuNPs) in prostate tumor therapy: green nanotechnology for production, in vivo tumor retention and evaluation of therapeutic efficacy, Dalton Trans. 46 (2017) 14561–14571.
[3] A.Y. Al-Yasiri, N.E. White, K.V. Katti, S.K. Loyalka, Estimation of tumor and local tissue dose in gold nanoparticles radiotherapy for prostate cancer, Rep. Practical Oncol. Radiother. 24 (2019) 288–293.
[4] E.B. Aladejana, C. Musara, Typha capensis (Rohrb.) N.E.Br. (Typhaceae): morphology, medicinal uses, biological and chemical properties, Plant Sci. Today. 7 (2020) 578–583.
[5] S.J. Amina, B. Guo, A review on the synthesis and functionalization of gold nanoparticles as a drug delivery vehicle, Int. J. Nanomed. 15 (2020) 9823–9857.
[6] H. Barabadi, M. Ovais, Z.K. Shinwari, M. Saravanan, Anti-cancer green bionanomaterials: present status and future prospects, Green Chem. Lett. Rev. 10 (2017) 285–314.
[7] T. Baruah, K. Hauneihkim, L. Kma, Naringenin sensitizes lung cancer NCI-H23 cells to radiation by downregulation of akt expression and metastasis while promoting apoptosis, Phcog. Mag. 16 (2020) 229.
[8] M. Bhia, M. Motallebi, B. Abadi, A. Zarepour, M. Pereira-Silva, F. Saremnejad, A. C. Santos, A. Zarrabi, A. Melero, S.M. Jafari, M. Shakibaei, Naringenin nano-delivery systems and their therapeutic applications, Pharmaceutics 13 (2021) 291.
[9] L. Biao, S. Tan, Q. Meng, J. Gao, X. Zhang, Z. Liu, Y. Fu, Green synthesis, characterization and application of proanthocyanidins-functionalized gold nanoparticles, Nanomaterials 8 (2018) 53.
[10] J.K. Campbell, J.L. King, M. Harmston, M.A. Lila, J.W. Erdman, Synergistic effects of flavonoids on cell proliferation in hepa-1c1c7 and LNCaP cancer cell lines, J. Food Sci. 71 (2006) S358–S363.
[11] Y. Choi, M. Choi, S. Cha, Y.S. Kim, S. Cho, Y. Park, Catechin-capped gold nanoparticles : green synthesis , characterization , and catalytic activity toward 4-nitrophenol reduction, Nanoscale Res. Lett. 9 (2014) 1–8.
[12] P. Dalwadi, P. Patani, I. Singhavi, Preparation and characterization of naringenin gold nano suspension for breast cancer, Int. Res. J. Pharm. 9 (2019) 128–133.
[13] N. Elahi, M. Kamali, M.H. Baghersad, Recent biomedical applications of gold nanoparticles: a review, Talanta 184 (2018) 537–556.
[14] A.M. Elbagory, C.N. Cupido, M. Meyer, A.A. Hussein, Large scale screening of southern African plant extracts for the green synthesis of gold nanoparticles using microtitre-plate method, Molecules 21 (2016).
[15] M.U. Farooq, V. Novosad, E.A. Rozhkova, H. Wali, A. Ali, A.A. Fateh, P.B. Neogi, A. Neogi, Z. Wang, Gold nanoparticles-enabled efficient dual delivery of anticancer therapeutics to HeLa cells, Sci. Rep. 8 (2018) 2907.
[16] M. Ferreira, D. Costa, Â. Sousa, Flavonoids-based delivery systems towards cancer therapies, Bioengineering 9 (2022) 197.
[17] S. Gera, S. Talluri, N. Rangaraj, S. Sampathi, Formulation and evaluation of naringenin nanosuspensions for bioavailability enhancement, AAPS PharmSciTech 18 (2017) 3151–3162.
[18] A.N. Geraldes, A.A. da Silva, J. Leal, G.M. Estrada-Villegas, N. Lincopan, K.V. Katti, A.B. Lug&atildeo, Green nanotechnology from plant extracts: synthesis and characterization of gold nanoparticles, Adv. Nanoparticles (2016) 176–185, 05.
[19] M. Gumustas, C.T. Sengel-Turk, A. Gumustas, S.A. Ozkan, B. Uslu, Effect of polymer-based nanoparticles on the assay of antimicrobial drug delivery systems, in: Multifunct. Syst. Comb. Deliv. Biosensing Diagnostics, Elsevier, 2017, pp. 67–108.
[20] V. Gupta, P. Trivedi, In vitro and in vivo characterization of pharmaceutical topical nanocarriers containing anticancer drugs for skin cancer treatment, in: Lipid Nanocarriers Drug Target, Elsevier, 2018, pp. 563–627.
[21] R. Henkel, W. Fransman, U.C. Hipler, C. Wiegand, G. Schreiber, R. Menkveld, F. Weitz, D. Fisher, Typha capensis (Rohrb.)N.E.Br. (bulrush) extract scavenges free radicals, inhibits collagenase activity and affects human sperm motility and mitochondrial membrane potential in vitro: a pilot study, Andrologia 44 (2012) 287–294.
[22] R. Henkel, W. Fransman, U.C. Hipler, C. Wiegand, G. Schreiber, R. Menkveld, F. Weitz, D. Fisher, Typha capensis (Rohrb.)N.E.Br. (bulrush) extract scavenges free radicals, inhibits collagenase activity and affects human sperm motility and mitochondrial membrane potential in vitro: a pilot study, Andrologia 44 (2012) 287–294.
[23] A. Ilfergane, Investigations on the Effects of Typha Capensis on Male Reproductive Functions, University of the Western Cape, 2016.
[24] A. Ilfergane, R.R. Henkel, Effect of Typha capensis (Rohrb.)N.E.Br. rhizome extract F1 fraction on cell viability, apoptosis induction and testosterone production in TM3-Leydig cells, Andrologia 50 (2018), e12854.
[25] K. Katti, N. Chanda, R. Shukla, A. Zambre, T. Suibramanian, R.R. Kulkarni, R. Kannan, K. V Katti, Green nanotechnology from cumin phytochemicals: generation of biocompatible gold nanoparticles, Int. J. Green Nanotechnol. Biomed. 1 (2009). B39–B52.
[26] K.V. Katti, Renaissance of nuclear medicine through green nanotechnology: functionalized radioactive gold nanoparticles in cancer therapy—my journey from chemistry to saving human lives, J. Radioanal. Nucl. Chem. 309 (2016) 5–14.
[27] K.V. Katti, M. Khoobchandani, V.C. Thipe, A.Y. Al-Yasiri, K.K. Katti, S.K. Loyalka, T.M. Sakr, A.B. Lugão, Prostate tumor therapy advances in nuclear medicine: green nanotechnology toward the design of tumor specific radioactive gold nanoparticles, J. Radioanal. Nucl. Chem. 318 (2018) 1737–1747.
[28] J. Kaur, M. Vyas, J. Singh, R. Prasad, J. Gupta, Therapeutic applications of naringenin, a flavanone enriched in citrus fruits, for disorders beyond diabetes, Phyton 89 (2020) 795–803.
[29] M. Khoobchandani, K.K. Katti, A.R. Karikachery, V.C. Thipe, D. Srisrimal, D. K. Dhurvas Mohandoss, R.D. Darshakumar, C.M. Joshi, K. V Katti, New approaches in breast cancer therapy through green nanotechnology and nano-ayurvedic medicine – pre-clinical and pilot human clinical investigations, Int. J. Nanomed. 15 (2020) 181–197.
[30] M. Khoobchandani, A. Khan, K.K. Katti, V.C. Thipe, A.Y. Al-Yasiri, D.K. D. MohanDoss, M.B. Nicholl, A.B. Lugão, C.P. Hans, K.V. Katti, Green nanotechnology of MGF-AuNPs for immunomodulatory intervention in prostate cancer therapy, Sci. Rep. 11 (2021), 16797.
[31] Y. Kita, T. Goto, S. Akamatsu, T. Yamasaki, T. Inoue, O. Ogawa, T. Kobayashi, Castration-resistant prostate cancer refractory to second-generation androgen receptor axis-targeted agents: opportunities and challenges, Cancers 10 (2018) 345.
[32] W. Lim, S. Park, F.W. Bazer, G. Song, Naringenin-induced apoptotic cell death in prostate cancer cells is mediated via the PI3K/AKT and MAPK signaling pathways, J. Cell. Biochem. 118 (2017) 1118–1131.
[33] W. Lim, S. Park, F.W. Bazer, G. Song, Naringenin-induced apoptotic cell death in prostate cancer cells is mediated via the PI3K/AKT and MAPK signaling pathways, J. Cell. Biochem. 118 (2017) 1118–1131.
[34] M. Movassaghi, R. Chung, C.B. Anderson, M. Stein, Y. Saenger, I. Faiena, Overcoming immune resistance in prostate cancer: challenges and advances, Cancers 13 (2021) 4757.
[35] S.K. Nune, N. Chanda, R. Shukla, K. Katti, R.R. Kulkarni, S. Thilakavathy, S. Mekapothula, R. Kannan, K.V. Katti, Green nanotechnology from tea: phytochemicals in tea as building blocks for production of biocompatible gold nanoparticles, J. Mater. Chem. 19 (2009) 2912–2920.
[36] S. Rajamani, A. Radhakrishnan, T. Sengodan, S. Thangavelu, Augmented anticancer activity of naringenin-loaded TPGS polymeric nanosuspension for drug

resistive MCF-7 human breast cancer cells, Drug Dev. Ind. Pharm. 44 (2018) 1752–1761.
[37] B. Salehi, P.V.T. Fokou, M. Sharifi-Rad, P. Zucca, R. Pezzani, N. Martins, J. Sharifi-Rad, The therapeutic potential of naringenin: a review of clinical trials, Pharmaceuticals 12 (2019) 1–18.
[38] W. Sangpheak, J. Kicuntod, R. Schuster, T. Rungrotmongkol, P. Wolschann, N. Kungwan, H. Viernstein, M. Mueller, P. Pongsawasdi, Physical properties and biological activities of hesperetin and naringenin in complex with methylated p-cyclodextrin, Beilstein J. Org. Chem. 11 (2015) 2763–2773.
[39] Y. Shi, L. Yang, M. Yu, Z. Li, Z. Ke, X. Qian, X. Ruan, L. He, F. Wei, Y. Zhao, Q. Wang, Seasonal variation influences flavonoid biosynthesis path and content, and antioxidant activity of metabolites in Tetrastigma hemsleyanum Diels & Gilg, PLoS One 17 (2022), e0265954.
[40] F.O. Shode, A.S. Mahomed, C.B. Rogers, Typhaphthalide and typharin, two phenolic compounds from Typha capensis, Phytochemistry 61 (2002) 955–957.
[41] R. Shukla, N. Chanda, A. Zambre, A. Upendran, K. Katti, R.R. Kulkarni, S.K. Nune, S.W. Casteel, C.J. Smith, J. Vimal, E. Boote, J.D. Robertson, P. Kan, H. Engelbrecht, L.D. Watkinson, T.L. Carmack, J.R. Lever, C.S. Cutler, C. Caldwell, R. Kannan, K. V. Katti, Laminin receptor specific therapeutic gold nanoparticles (198 AuNP-EGCg) show efficacy in treating prostate cancer, Proc. Natl. Acad. Sci. USA 109 (2012) 12426–12431.
[42] M. Shulman, M. Cohen, A. Soto-Gutierrez, H. Yagi, H. Wang, J. Goldwasser, C. W. Lee-Parsons, O. Benny-Ratsaby, M.L. Yarmush, Y. Nahmias, Enhancement of naringenin bioavailability by complexation with hydroxypropoyl-β-cyclodextrin, PLoS One 6 (2011).
[43] N.R.S. Sibuyi, V.C. Thipe, K. Panjtan-Amiri, M. Meyer, K. V Katti, Green synthesis of gold nanoparticles using Acai berry and Elderberry extracts and investigation of their effect on prostate and pancreatic cancer cells, Nanobiomedicine 8 (2021) 1–8.
[44] A. Stasiłowicz-Krzemień, M. Gołębiewski, A. Płazińska, W. Płaziński, A. Miklaszewski, M. Żarowski, Z. Adamska-Jernaś, J. Cielecka-Piontek, The systems of naringenin with solubilizers expand its capability to prevent neurodegenerative diseases, Int. J. Mol. Sci. 23 (2022) 755.
[45] R. Sultan, N. Majid, S. Nissar, A. Rather, Seasonal variation of phytochemicals, Int. J. Pharm. 8 (2018) 987–990.
[46] L. Sun, S. Pu, J. Li, J. Cai, B. Zhou, G. Ren, Q. Ma, L. Zhong, Size controllable one step synthesis of gold nanoparticles using carboxymethyl chitosan, Int. J. Biol. Macromol. 122 (2019) 770–783.
[47] H. Sung, J. Ferlay, R.L. Siegel, M. Laversanne, I. Soerjomataram, A. Jemal, F. Bray, Global cancer statistics 2020: GLOBOCAN estimates of incidence and mortality worldwide for 36 cancers in 185 countries, CA, Cancer J. Clin. 71 (2021) 209–249.
[48] M.Y. Teo, D.E. Rathkopf, P. Kantoff, Treatment of advanced prostate cancer, Annu. Rev. Med. 70 (2019) 479–499.
[49] V.C. Thipe, K.P. Amiri, P. Bloebaum, A.K. Raphael, M. Khoobchandani, K.K. Katti, S.S. Jurisson, K.V. Katti, Development of resveratrol-conjugated gold nanoparticles: interrelationship of increased resveratrol corona on anti-tumor efficacy against breast, pancreatic and prostate cancers, Int. J. Nanomed. 14 (2019) 4413–4428.
[50] V.C. Thipe, A.R. Karikachery, P. Çakılkaya, U. Farooq, H.H. Genedy, N. Kaeokhamloed, D.-H. Phan, R. Rezwan, G. Tezcan, E. Roger, K.V. Katti, Green nanotechnology—an innovative pathway towards biocompatible and medically relevant gold nanoparticles, J. Drug Deliv. Sci. Technol. 70 (2022), 103256.
[51] V.C. Thipe, M. Keyster, K.V. Katti, Sustainable Nanotechnology: Mycotoxin Detection and Protection, 2018, pp. 323–349.
[52] F. Wang, Y.-C. Wang, S. Dou, M.-H. Xiong, T.-M. Sun, J. Wang, Doxorubicin-tethered responsive gold nanoparticles facilitate intracellular drug delivery for overcoming multidrug resistance in cancer cells, ACS Nano 5 (2011) 3679–3692.
[53] M. Yafout, A. Ousaid, Y. Khayati, I.S. El Otmani, Gold nanoparticles as a drug delivery system for standard chemotherapeutics: a new lead for targeted pharmacological cancer treatments, Sci. African. 11 (2021), e00685.
[54] L. Yang, K.-S. Wen, X. Ruan, Y.-X. Zhao, F. Wei, Q. Wang, Response of plant secondary metabolites to environmental factors, Molecules 23 (2018) 762.